Proceedings of 14th IOE Graduate Conference
Peer Reviewed
Year: 2023 Month: December Volume: 14
ISSN: 2350-8914 (Online), 2350-8906 (Print)

Flood Hazard Assessment of the East Rapti River Basin under Climate Change Scenario

Sneha Sanjel [a], Suraj Lamichhane [b]

[a, b] *Department of Civil Engineering, Pulchowk Campus, IOE, Tribhuvan University, Nepal*
[a] snehasanjel117@gmail.com, [b] klsuraj@gmail.com

Abstract
Frequent occurrences of flooding in Nepal have inflicted significant damage to both property and human lives, particularly in the lowland areas. This comprehensive study aims to assess the flood hazards within the East Rapti River Basin. This assessment is carried out in the context of the latest CMIP6 (Coupled Model Intercomparison Project) climate change projections. To conduct this analysis, HEC RAS 2D rain-on-grid modeling was used for flood analysis, followed by post-processing in QGIS. The integration of CMIP6 climate data focused on shared socioeconomic pathways (SSPs), SSP2-4.5 and SSP5-8.5 scenarios, with a particular emphasis on improving model accuracy through bias correction of precipitation data. Various return period data were calculated using statistical methods, leading to the preparation of detailed flood hazard maps for both 50-year and 100-year return periods for exisitng as well as for future scenarios. These maps provide valuable insights by comparing flood hazards in both existing and future scenarios, reflecting the changing climate conditions. The flood hazard assessment classifies hazards based on water depth, identifying regions susceptible to flooding. The comparative assessment undertaken in this study shows the anticipated increase in flooding extent in the future years. The result shows that under the SSP2-4.5 and SSP5-8.5 future scenarios, the extreme hazard extent for the 50-year return period is expected to rise by 1.49 and 1.706 times, respectively, compared to the existing scenario. Moreover, for the 100-year return period, these scenarios project even more substantial increase, with an estimated rise of 1.71 and 2.02 times, respectively, in comparison to the exisitng scenario. By integrating hydraulic modeling, climate change projections, and flood hazard assessments, this study aims to provide insights essential for flood management planning. The results obtained from this research, coupled with the prepared maps, introduce a powerful tool for the visualization and quantification of flood hazards. These findings serve as a valuable resource for decision-makers, equipping them with a deeper understanding of emerging challenges and facilitating well-informed actions to address the evolving flood risks.

Keywords
Flood Hazard, Climate Change Projections, Coupled Model Intercomparison Project Phase 6 (CMIP6), HEC-RAS, Rain-on-Grid Model

1. Introduction

Flood is a common hazard causing significant damage and loss of lives worldwide. The damages caused by flood has intensified in the recent years. Every year, following the monsoon rain, flood affects the livelihood of people residing in the Terai region of Nepal [1]. Nepal faces a spectrum of water-related disasters of different degree of severity and scale. These calamities, originating from water-related causes, exert their influence on multiple regions within the country on a regular basis. The major cause behind the recurring scenario is the monsoonal precipitation, which predominantly occurs between the months of June and September [2]. Flooding results in the damage of structures and property losses, causes multiple fatalities and affects the livelihood of many, requiring critical planning for flood hazard mapping. Flooding in the East Rapti river basin ranges from prone to flash floods in the upper parts to a more delayed but sustained floods in the lower parts. The re- occurrence of East Rapti river flooding have had devastating effects in the past [3]. During the pre-monsoon period, the basin witnesses an approximate rainfall of 150 mm, followed by a substantial increase to around 2000 mm throughout the monsoon season. Subsequently, the post-monsoon phase experiences a decrease to about 80 mm of rainfall, while the winter season receives 20 mm of precipitation [4].

Climate change is anticipated to have notable impacts on flooding, in terms of both frequency and severity of floods. For studying about flood hazards in the future, considering the effects of climate change is particularly important. [5]. According to the IPCC, the Earth's temperature in 2021 reached its highest point in the last 2000 years. This 1.5-degree temperature increase has led to significant alterations in weather patterns, the melting of polar ice caps, shifts in precipitation trends, and the subsequent rise in climate-induced disasters. The study of climate change and flooding in South Asia by Mirza, 2011 [6] shows that even though high flooding of the past was in between the range of climate variability, in the future, the situation will not be the same and the magnitude and extent of flooding will increase because of the effects of climate change. According to present climate change forecasts, it is expected that the Hindu Kush Himalayan area will experience a higher occurrence of extreme climate events due to the rise in intense rainfall incidents. This shows the need for proactive strategies to reduce their consequences and strengthen resilience [1].

Studying flood hazards is beneficial for policymakers and planners as it assists in determining the crucial areas for creating flood management strategies in the future [7]. With

the increase in flooding and their adverse affects on livelihood, it has become significant to identify and map flood hazards. Given the inevitability of losses caused by floods, flood hazard mapping as a highly effective approach for mitigating and preventing such events [8]. In the past, 1D hydraulic models have been commonly utilized for analyzing floods. However, due to the limitations of 1D models in flat terrains, many of these models are now being substituted with 2D hydraulic models to improve performance and accuracy [9]. There have been multiple studies of flood hazard using HEC-RAS. The study along Daraudi river basin uses HEC RAS and ArcGIS for flood hazard mapping, utilizing 1D steady flow analysis. The study indicate a rise in inundation area with higher peak discharge and it suggests on using 2D unsteady flow for assessing natural river systems [10]. The Lothar Khola basin was studied using HEC RAS, utilizing recorded precipitation and river flow data [11]. Flood hazard mapping and vulnerability analysis was done for the Bishnumati River with the use of HEC RAS and GIS. The resulting hazard map highlighted the extent of inundation, revealing urban and cultivated lands as particularly susceptible areas [2]. Study conducted in the southern region of the Himalayas, applied the HEC-RAS model to generate a detailed flood inundation map, facilitating an analysis of flood hazard [12]. Grid-based rainfall modeling, often referred to as rain-on-grid modeling, is a modeling approach used for simulating and studying rainfall distributions over a geographical area. This approach involves dividing the overall study region into a grid or mesh composed of individual cells. Each cell is then provided with a specific rainfall information, representing the local differences in precipitation. The Rain on Grid method in HEC-RAS holds advantages over traditional models, allowing for detailed representation of rainfall and runoff variability. This leads to more accurate flood risk estimates and informed management decisions [13]. Using the rain-on-grid or the direct rainfall method in HEC RAS generated thorough satisfactory flood inundation maps. Comparing it with other approaches, this approach was able to generate better the flow processes and direction of runoff within a specific catchment area [14].

This study aims to evaluate the comprehensive flood hazard within the context of climate change scenarios in the East Rapti river basin. This includes firstly, developing a hydraulic model to assess both present and future flooding scenarios in the study area considering climate change projections; and secondly, conducting an analysis of flood hazards for different return period floods.

2. Materials and Methods

2.1 Study Area

The East Rapti river basin lies in the central Nepal, Bagmati province, passes through Makawanpur and Chitwan districts and is a sub-basin of Narayani River system. The basin extends from latitude 27° 21' 23" N to 27° 47' 00" N and longitude 84° 08' 43"E to 85° 11' 57" E. Chitwan district holds about 56% of the river basin's area, and Makawanpur district holds about 44% of it. The area is approximately 3200sq.km. The elevation ranges from 2584m as the highest in upstream region and 124m as the lowest in downstream region. The East Rapti river basin receives a rainfall of roughly 150 mm in pre-monsoon, 2000 mm in monsoon, 80 mm in post-monsoon, and 20 mm during the winter season [4]. The basin includes 32 Village Development Committees (VDCs) from Chitwan district and 23 out of 43 VDCs from Makawanpur districts. Based on the land classification data obtained from ICIMOD, forest covers majority of the area in this river basin, followed by cropland. According to CBS, agriculture is the most dominant occupation in this region. The combined effects of river action and gravity have resulted in a wide range of landforms and soil types in the region. The hilly terrain features steep slopes and a mix of alluvial plains, while the climate and topography contribute to diverse soil compositions. In the sloping areas, soils can range from sandy or cobbly to sandy and loamy skeletal, whereas the plains consist of coarse and fine loamy soils [15].

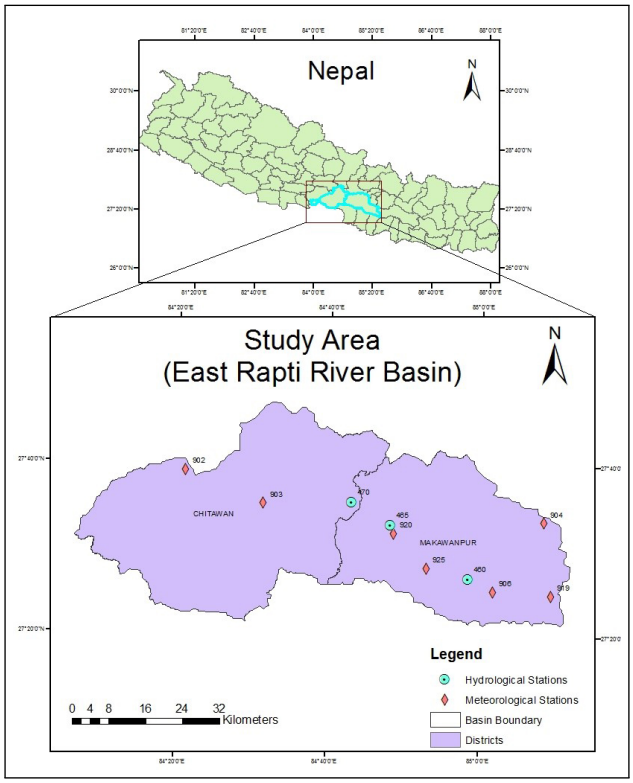

Figure 1: Location Map of the Study Area [16]

2.2 Methodological Framework

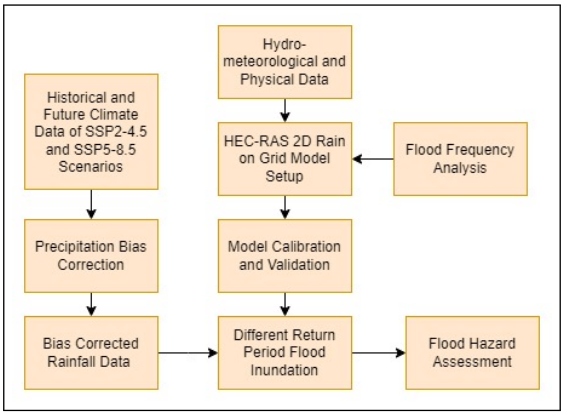

Figure 2: Methodological Framework of the Study

The primary data required for modeling was acquired from different sources. The hydro-meteorological data including the precipitation data and discharge data was collected from the Department of Hydrology and Meteorology (DHM), Nepal. The DEM of 30m and land classification data was downloaded from open source websites, including the Copernicus website and ICIMOD website respectively.

2.2.1 Return Period Calculation

Flood frequency analysis was performed using statistical analysis methods such as Gumbel's method, Log Pearson Type III method and Log Normal method for different return periods. Upon analyzing the results, the method that demonstrated the highest reliability for further analysis was selected. Statistical indicators were used to determine the best fit method using Chi-Square test, Kolmogorov Smirnov test and the Anderson Darling test. Based upon the best fit test, Log Pearson III distribution was used for flood frequency analysis.

2.2.2 HEC-RAS Rain-on-Grid Modeling

The hydraulic modeling in this study was conducted using HEC RAS 6.3.1. Rain-on-grid or direct rainfall modeling approach was used for hydraulic analysis. This involved the division of the entire study area into a grid or mesh consisting of individual cells.

Precipitation data was used as the unsteady flow data input in the model. The precipitation data obtained from DHM contains point dataset. However, the data for the whole catchment area is required in order to conduct flood analysis. The average precipitation data required for the analysis was computed using the thiessen polygon method. The thiessen polygon method works by providing a weightage to each station according to the area around it. The average precipitation data required for the analysis was thus computed using this method. The meteorological stations were plotted using the meteorological data input in the unsteady flow data file. Manning's roughness coefficient was prepared using the imported land classification data layer from ICIMOD and manning's n table was determined from the HEC RAS manual. The value of manning's roughness coefficient was adjusted according to the land classification and the model was run multiple times to get the required ground results.

Table 1: Manning's Roughness Values

Land Classification	Manning's n	% Impervious
Waterbody	0.035	90
Grassland	0.045	5
Forest	0.13	8
Riverbed	0.03	30
Builtup Area	0.08	85
Cropland	0.05	5
Bare Soil	0.025	8
Other Wooded Land	0.04	15

Breakline was created along the river channel throughout the basin. Diffusive wave equation was used as the calculation equation set option for modeling. Courant condition was used for the time step with 1 minute as computation interval. Using courant condition is considered to be the most effective way to estimate computational time setup. The result was then calibrated and validated by the comparison of simulated discharge and observed discharge from the station Rajaiya. NSE, R^2, PBIAS, RSR values were calculated for multiple years for calibrating and validating the model. Model calibration was done for the years 2006, 2007, 2009 and 2010 and model validation was done for the years 2011, 2012, 2018 and 2019.

2.2.3 Future Climate Projection

In this Study, 5 Global Climate Models (GCMs) under CMIP6 (Coupled Model Intercomparison Project Phase 6) was used. The selection of Global Climate Models (GCMs) was based on the availability of historical and future daily rainfall data for both SSP2-4.5 and SSP5-8.5 scenarios, with a predominant usage in the South Asian region. The five GCM's used in this study are ACCESS, EARTH, MIROC, MPI and MRI [17]. These GCM's were used for two Shared Socio-economic Pathways (SSPs), SSP2-4.5 and SSP5-8.5 scenarios. SSP5-8.5 envisions a world with heightened fossil fuel usage and swift economic growth, resulting in elevated greenhouse gas emissions and a radiative forcing trend of about 8.5 watts per square meter (W/m²) by 2100. In SSP 2-4.5, a future emerges with moderated greenhouse gas emissions, yielding a radiative forcing trajectory of around 4.5 watts per square meter (W/m²) by 2100 [18].

In order to improve the reliability and fix the possible errors in the models, the future rainfall projections obtained for seven stations within the study area were bias corrected using RQUANT approach. To select the best-suited GCM for further analysis, thiessen polygons was used to calculate the area of influence of each station, and their corresponding weights were established. These weights were used to scale the station indicators for each GCM, resulting in single indicator values for each GCM. Based on the statistical indicators, only the bias corrected rainfall data obtained from MIROC was selected for further analysis. The bias corrected precipitation data of the seleted GCM for both the SSP scenarios, SSP2-4.5 and SSP5-8.5 was then used for calculation of future different years return period flood.

Table 2: Statistical Indicator Values for Different GCM

GCM	Indicators		
	NSE	PBIAS	R^2
ACCESS	0.9561	7.6024	0.988
EARTH	0.9464	-3.9357	0.965
MIROC	0.9693	2.188	0.9887
MPI	0.9691	-2.5179	0.9812
MRI	0.9689	0.2268	0.9859

2.2.4 Flood Hazard Assessment

Identifying flood genesis factor is of utmost importance when conducting hazard assessment. Flood depth serves as the crucial factor for assessing the extent of damage and computing the hazard associated with flooding. The flood hazard assessment generally looks at the extent and depth of flooding and flood depth is considered to be the most important factor while looking at flood hazard [19]. The

process of mapping and evaluating the flood hazards helps in identifying the regions that are prone to flooding which will further enhance the management of flood risks. The occurrence of flooding in any area can be considered a hazard itself, but the occurrences of flood can be categorized according to the severity, according to the depth of flooding.

This study classifies hazard into four categories.The categorization used in this study is based on water depth, with classifications as follows: depth less than 1m as low, depths ranging from 1 to 2m as moderate, depths from 2 to 3m as significant, and depth exceeding 3m as extreme hazard levels [3, 10, 20].

3. Results and Discussion

3.1 HEC-RAS Rain-on-Grid Model

The efficiency of the model calibration and validation can be analyzed using various statistical equations. The calibration and validation of the model was done by the use of statistical parameters including, Nash-Sutcliffe efficiency (NSE), Percent bias (PBIAS), Coefficient of determination (R^2), Standard deviation ratio (RSR). Table 3 shows the calibration and validation results.

Table 3: HEC-RAS Model Performance

Phase	Year	NSE	R^2	PBIAS	RSR
Calibration	2006	0.709	0.769	1.06	0.539
	2007	0.819	0.842	-0.025	0.425
	2009	0.518	0.519	1.201	0.693
	2010	0.82	0.848	1.214	0.424
Validation	2011	0.824	0.857	-0.087	0.419
	2012	0.925	0.926	-3.493	0.273
	2018	0.688	0.905	-3.355	0.558
	2019	0.765	0.806	0.123	0.483

The calibration and validation results show NSE values ranging from 0.518 to 0.82 and 0.688 to 0.925, R^2 values ranging from 0.519 to 0.848 and 0.806 to 0.926, PBIAS values ranging from -0.025 to 1.214 and -0.087 to -3.493, and RSR values ranging from 0.424 to 0.693 and 0.273 to 0.558.

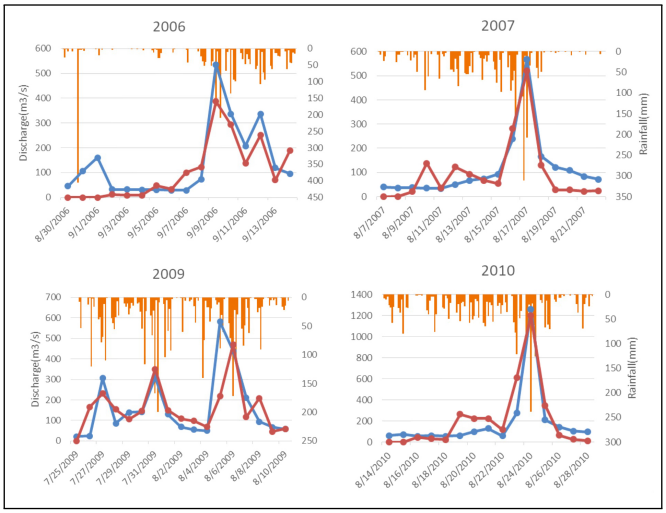

Figure 3: Observed and Simulated Discharge for Calibration Period

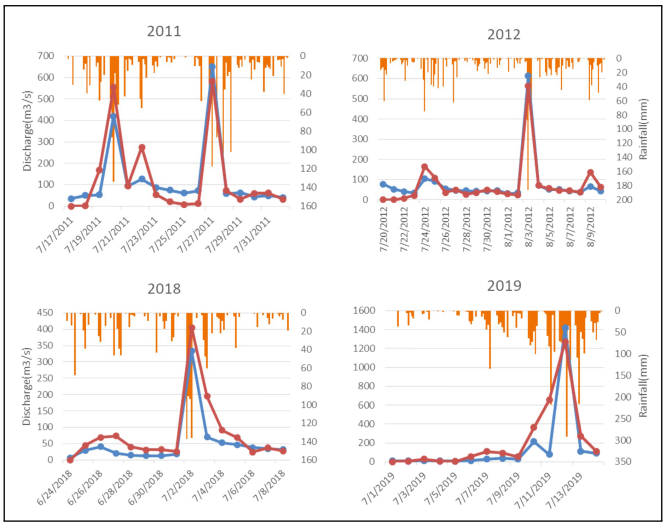

Figure 4: Observed and Simulated Discharge for Validation Period

The values for validation phase seems to have better relation as compared to calibration phase. However, the values of statistical parameters for both phases obtained after calculation shows that the model performance is satisfactory [21]. All of these values for NSE, PBIAS, R^2 and RSR are within the acceptable limit and they show a close alignment between the observed and simulated values, with minimal dispersion.

3.2 Return Period Data Calculation

Various statistical methods including, Gumbel's method, Log Pearson Type III and Log Normal method was used for the calculation of return period data. The daily precipitation data form seven meteorological stations were analyzed to calculate the basin average rainfall with the use of thiessen polygon method. One day maximum annual rainfall was then calculated, which was then used in statistical calculations. Return period data was calculated for historical and future scenario for SSP2-4.5 and SSP5-8.5.

Followed by return period calculation, goodness of fit test was run to determine the best fit distribution among all. Statistical indicators were used to determine the best fit method using Chi-Square test, Kolmogorov Smirnov test and the Anderson Darling test. Based on the results obtained in statistical tests, and the value from Log Pearson III being higher than that of the other methods, Log Pearson III distribution was chosen.

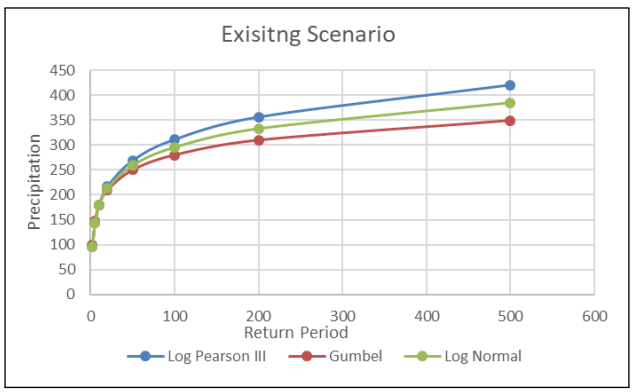

Figure 5: Return Period Calculation for Existing Scenario

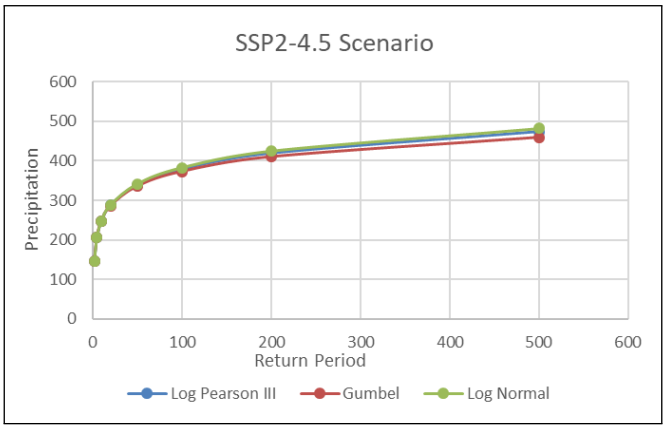

Figure 6: Return Period Calculation for SSP245 Scenario

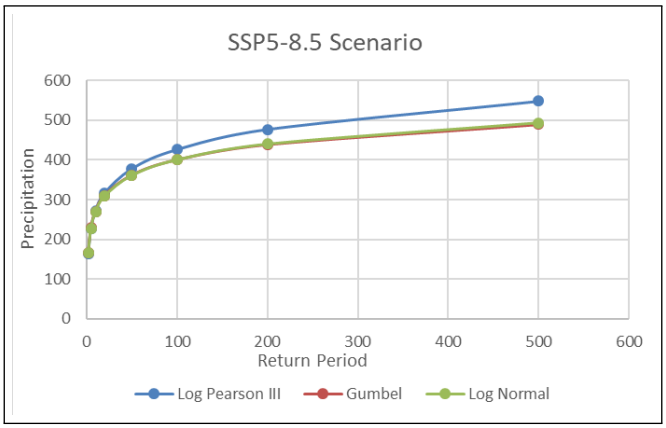

Figure 7: Return Period Calculation for SSP585 Scenario

Table 4: Best Fit Test for Existing Scenario

Distribution Method	Kolmogorov Smirnov		Chi-Square		Anderson Darling	
	Statistics	**Rank**	**Statistics**	**Rank**	**Statistics**	**Rank**
Log Pearson III	0.12	1	7.6	1	0.27	1
Gumbel	0.13	2	7.6	2	0.423	2
Log Normal	0.149	3	7.6	3	0.293	3

Table 5: Best Fit Test for SSP245 Scenario

Distribution Method	Kolmogorov Smirnov		Chi-Square		Anderson Darling	
	Statistics	**Rank**	**Statistics**	**Rank**	**Statistics**	**Rank**
Log Pearson III	0.094	2	0.8	1	0.287	1
Gumbel	0.1	3	2.8	3	0.312	3
Log Normal	0.092	1	0.8	2	0.283	2

Table 6: Best Fit Test for SSP585 Scenario

Distribution Method	Kolmogorov Smirnov		Chi-Square		Anderson Darling	
	Statistics	**Rank**	**Statistics**	**Rank**	**Statistics**	**Rank**
Log Pearson III	0.072	1	0.4	1	0.158	1
Gumbel	0.083	2	0.4	2	0.217	2
Log Normal	0.08	3	0.4	3	0.198	3

3.3 Future Flow Projection

The range of annual projected precipitation ranges from 1275.16mm to 3310.497mm for SSP2-4.5 and 1103.606mm to 3756.742mm for SSP5-8.5. SSP5-8.5 projects a higher rainfall in comparison to SSP2-4.5 The graph illustrates a rise in annual maximum precipitation when comparing future projected data to historical data, indicating a potential increase in intensity of future flooding.

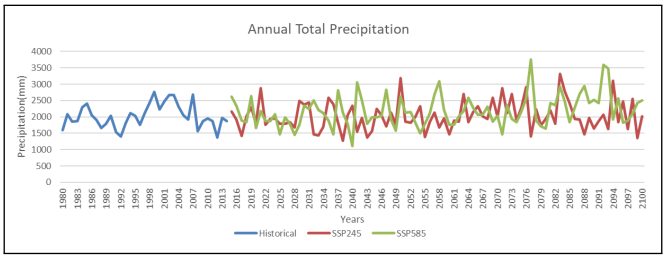

Figure 8: Historical and Future Annual Total Precipitation for different Scenarios

3.4 Flood Hazard Assessment

Depth of flooding is considered as the primary evaluation criteria [22] for determining the hazards for existing and future scenarios for different return periods. Flood hazard analysis for both the present and future flooding scenario was classified into four hazard classification. The summary of the extent of hazard of the study area for 50 year and 100 year return period is as shown in the tables.

Table 7: Flood Hazard for 50-year Return Period

Hazard Class	Existing		SSP245		SSP585	
	Area (km^2)	%	Area (km^2)	%	Area (km^2)	%
<1m	222.4909	50.96%	221.8523	43.27%	219.5856	40.69%
(1-2)m	85.3738	19.55%	100.4191	19.58%	106.1388	19.67%
(2-3)m	41.93617	9.60%	60.499	11.80%	65.74546	12.18%
>3m	86.83639	19.89%	129.977	25.35%	148.1982	27.46%
Total	436.6373	100.00%	512.7474	100.00%	539.6681	100.00%

Table 8: Flood Hazard for 100-year Return Period

Hazard Class	Existing		SSP245		SSP585	
	Area (km^2)	%	Area (km^2)	%	Area (km^2)	%
<1m	223.6027	49.67%	217.3429	39.36%	211.0102	36.07%
(1-2)m	88.76721	19.72%	108.1077	19.58%	112.6932	19.26%
(2-3)m	45.06651	10.01%	67.88723	12.29%	73.24869	12.52%
>3m	92.70248	20.59%	158.826	28.76%	188.0141	32.14%
Total	450.1389	100.00%	552.1638	100.00%	584.9662	100.00%

The result shows the extent of areas that fall under different hazard classification. Looking at the data of 50 year return period, it is evident that the inundation area is highest in low flood hazard classification. However, for future scenario, in both SSP 2-4.5 and SSP5-8.5, the region of extreme flood is seen to be increasing drastically. Given that SSP5-8.5 exhibited higher precipitation in climate projection, it suggests a likelihood of an increase in the flooded area within the floodplain, for both low and severe hazard scenarios.

The extent of inundation areas exhibits notable changes. For a 50-year return period, the total inundated area percentage for

extreme hazard increases from 19.8% in the existing scenario to 25.3% and 27.4% in the future SSP 2-4.5 and SSP5-8.5 scenarios respectively. A similar trend is observed for the 100-year return period. In the existing scenario, during a 100-year return period, low flood covers 49.6% of the area, while extreme flood encompasses 20.59%. However, in the future SSP 2-4.5 and SSP 5-8.5 scenario, low flood coverage decreases to 39.36% and 36.07% respectively, while extreme flood area increases to 28.76% and 32.14% respectively.

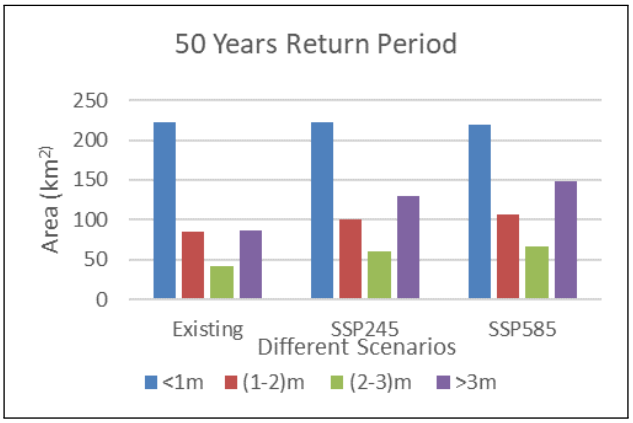

Figure 9: Hazard Extent for Existing and Future Scenarios for 50year Return Period

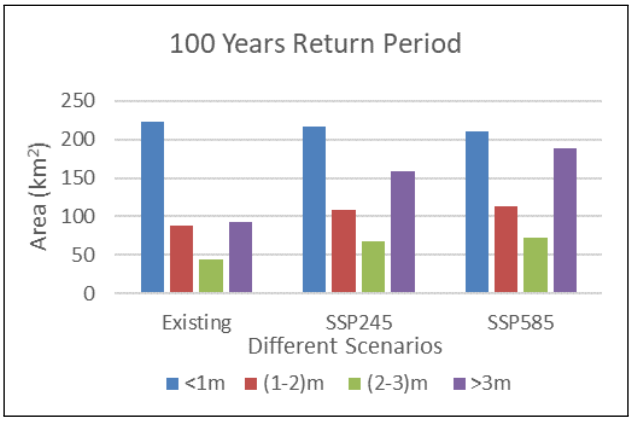

Figure 10: Hazard Extent for Existing and Future Scenarios for 100year Return Period

The result shows that the extent of severe hazard of future scenario SSP 2-4.5 and SSP5-8.5 increased by 1.49 times and 1.706 times that of existing scenario for 50 years return period. Similarly, for 100 years return period, the result shows that the extent of severe hazard of future scenario SSP2-4.5 and SSP5-8.5 increased by 1.71 times and 2.02 times that of existing scenario. The total inundated area has thus increased by more than 100sq.km. The intensity of flooding events with a 100year return period appears to escalate in both the current and future scenarios. Study by Shrestha, 2019, also indicate that the flood hazard zones could escalate due to the effects of climate change [23]. Similarly, the effects of climate change on flood hazard is assumed to extend even beyond the river basin level to a global scale [24]. This suggests a probable concerning trend where the severity of such flooding incidents may become more profound, highlighting the need for proactive measures and comprehensive strategies to mitigate their impacts and enhance resilience.

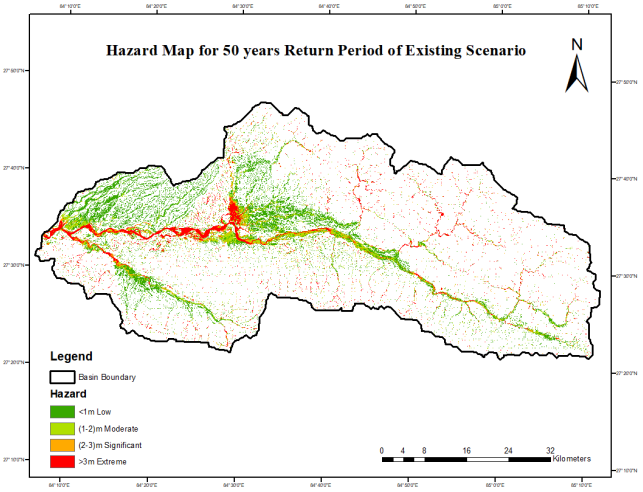

Figure 11: Hazard Maps for 50 Year Return Period of Existing Scenario

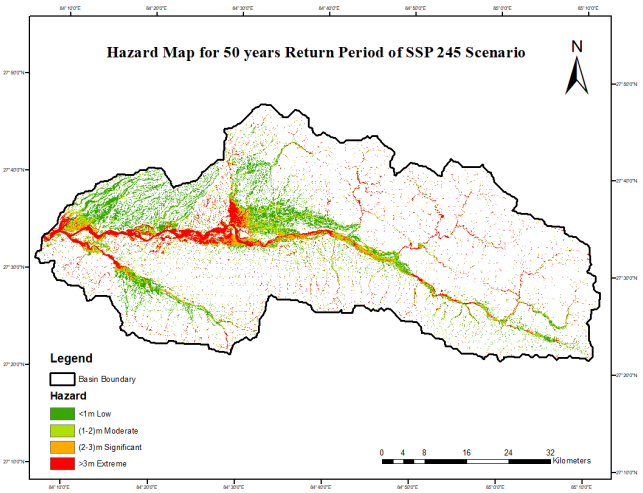

Figure 12: Hazard Maps for 50 Year Return Period of SSP2-4.5 Scenario

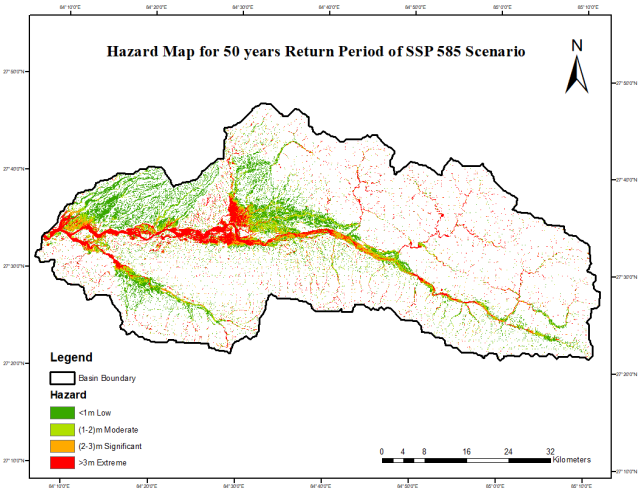

Figure 13: Hazard Maps for 50 Year Return Period of SSP5-8.5 Scenario

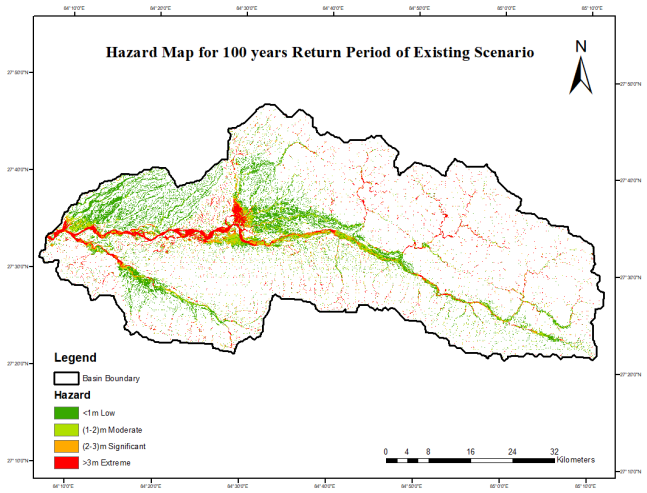

Figure 14: Hazard Maps for 100 Year Return Period of Existing Scenario

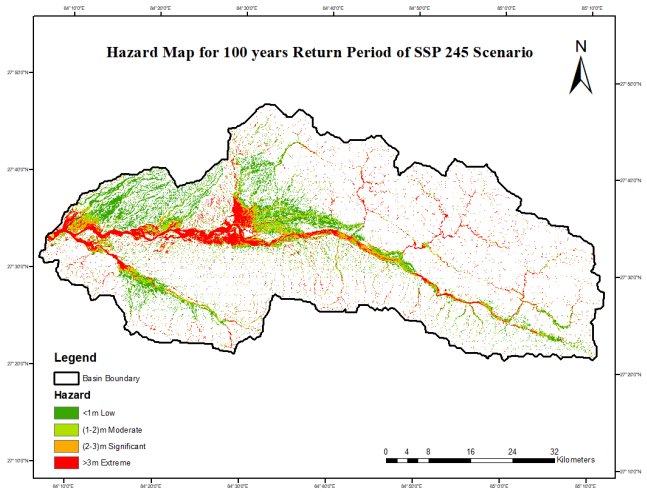

Figure 15: Hazard Maps for 100 Year Return Period of SSP2-4.5 Scenario

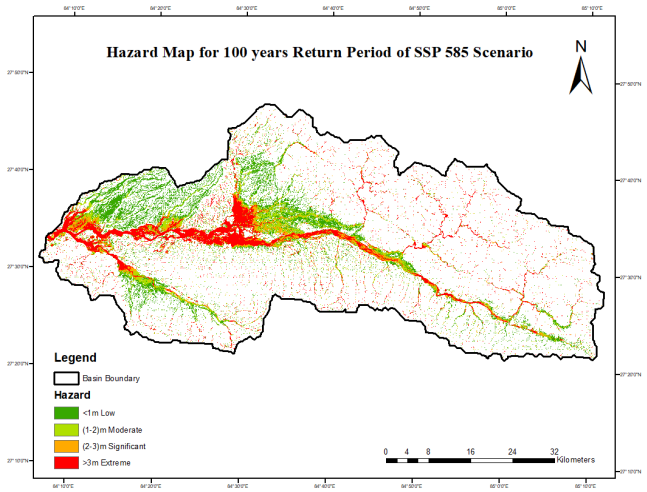

Figure 16: Hazard Maps for 100 Year Return Period of SSP5-8.5 Scenario

4. Conclusion

This study conducted flood hazard assessment of the East Rapti River Basin under CMIP6 climate change projections. For flood analysis, HEC RAS 2D rain on grid modeling or the direct rainfall approach was used. CMIP6 climate data for SSP2-4.5 and SSP5-8.5 scenarios were used for climate change projections. Precipitation bias correction was done to obtain bias corrected precipitation data. Flood frequency analysis was conducted and flood hazard maps for probable return period of 50years and 100 years were prepared. The maps prepared were for existing scenario and for SSP2-4.5 and SSP5-8.5 future scenarios. The HEC RAS model calibration and validation using different statistical indicators including NSE, PBIAS, R^2 and RSR show that the obtained values are in acceptable range and that the model has been calibrated and validated.

For the return period data calculation, Log Pearson III was found to be the most appropriate one based on the best fit test. The assessment of hazard maps for different scenario show that flooding in the future climate scenario will likely increase as compared to the existing scenario. It was observed that for 100 years return period extreme hazard class increased from 20.5% to 32.14% and 28.7%, and low class hazard decreased from 49.6% to 36.07% and 39.3% from existing to future SSP5-8.5 and SSP2-4.5 scenario respectively. The result shows that the low hazard class has not decreased much but there is a significant amount of total hazard area difference in extreme hazard zone when comparing existing and future scenarios. The results indicate that the extent of extreme hazard in future scenarios SSP2-4.5 and SSP5-8.5 increased by 1.49 times and 1.706 times for the 50-year return period, and by 1.71 times and 2.02 times for the 100-year return period, respectively, in comparison to the existing scenario.The results obtained and illustrated in map form introduces an approach to visualizing and quantifying flood hazard and vulnerability, thereby helping decision-makers in understanding the challenges and facilitating the necessary actions to be taken.

Acknowledgments

The authors would like to thank the Department of Hydrology and Meteorology (DHM), International Centre for Integrated Mountain Development (ICIMOD), and Government of Nepal for providing necessary data required for the study.

References

[1] Til Prasad Pangali Sharma, Jiahua Zhang, Narendra Raj Khanal, Foyez Ahmed Prodhan, Lkhagvadorj Nanzad, Da Zhang, and Pashupati Nepal. A geomorphic approach for identifying flash flood potential areas in the east rapti river basin of nepal. *ISPRS International Journal of Geo-Information*, 10(4):247, 2021.

[2] Susheel Dangol and Arnob Bormudoi. Flood hazard mapping and vulnerability analysis of bishnumati river, nepal. *Journal on Geoinformatics, Nepal*, 14:20–24, 2015.

[3] Roshika Bhattarai, Utsav Bhattarai, Vishnu Prasad Pandey, and Pawan Kumar Bhattarai. An artificial neural network-hydrodynamic coupled modeling approach to assess the

impacts of floods under changing climate in the east rapti watershed, nepal. *Journal of Flood Risk Management*, 15(4):e12852, 2022.

[4] Ramchandra Karki, Shabeh ul Hasson, Udo Schickhoff, Thomas Scholten, and Jürgen Böhner. Rising precipitation extremes across nepal. *Climate*, 5(1):4, 2017.

[5] Binata Roy, Md Sabbir Mostafa Khan, AKM Saiful Islam, Md Jamal Uddin Khan, and Khaled Mohammed. Integrated flood risk assessment of the arial khan river under changing climate using ipcc ar5 risk framework. *Journal of Water and Climate Change*, 12(7):3421–3447, 2021.

[6] M Monirul Qader Mirza. Climate change, flooding in south asia and implications. *Regional environmental change*, 11(Suppl 1):95–107, 2011.

[7] Phong Tran, Rajib Shaw, Guillaume Chantry, and John Norton. Gis and local knowledge in disaster management: a case study of flood risk mapping in viet nam. *Disasters*, 33(1):152–169, 2009.

[8] Saraswati Thapa, Anup Shrestha, Suraj Lamichhane, Rabindra Adhikari, and Dipendra Gautam. Catchment-scale flood hazard mapping and flood vulnerability analysis of residential buildings: The case of khando river in eastern nepal. *Journal of Hydrology: Regional Studies*, 30:100704, 2020.

[9] Venkatesh Merwade, Aaron Cook, and Julie Coonrod. Gis techniques for creating river terrain models for hydrodynamic modeling and flood inundation mapping. *Environmental Modelling & Software*, 23(10-11):1300–1311, 2008.

[10] Pratibha Banstola, P Krishna, and B Sapkota. Flood risk mapping and analysis using hydrodynamic model hec-ras: A case study of daraudi river, chhepatar, gorkha, nepal. *Journal of Natural Resources*, 2(3):25–44, 2019.

[11] Bikram Manandhar. Flood plain analysis and risk assessment of lothar khola. *Master of Science Thesis in Watershed Management. Tribhuvan University Institute of Forestry Pokhara, Nepal*, 2010.

[12] Dibit Aryal, Lei Wang, Tirtha Raj Adhikari, Jing Zhou, Xiuping Li, Maheswor Shrestha, Yuanwei Wang, and Deliang Chen. A model-based flood hazard mapping on the southern slope of himalaya. *Water*, 12(2):540, 2020.

[13] Sean J Zeiger and Jason A Hubbart. Measuring and modeling event-based environmental flows: An assessment of hec-ras 2d rain-on-grid simulations. *Journal of Environmental Management*, 285:112125, 2021.

[14] Amrei David and Britta Schmalz. Flood hazard analysis in small catchments: Comparison of hydrological and hydrodynamic approaches by the use of direct rainfall. *Journal of Flood Risk Management*, 13(4):e12639, 2020.

[15] Bryan Randolph Bruns, Don Jayatissa Bandaragoda, and M Samad. *Integrated water-resources management in a river-basin context: institutional strategies for improving the productivity of agricultural water management*. IWMI, 2002.

[16] Department of Survey, Government of Nepal. Shapefile/GIS Data for Political and Administrative Map of Nepal, 2020.

[17] Vimal Mishra, Udit Bhatia, and Amar Deep Tiwari. Bias-corrected climate projections for south asia from coupled model intercomparison project-6. *Scientific data*, 7(1):338, 2020.

[18] Brian C O'Neill, Claudia Tebaldi, Detlef P Van Vuuren, Veronika Eyring, Pierre Friedlingstein, George Hurtt, Reto Knutti, Elmar Kriegler, Jean-Francois Lamarque, Jason Lowe, et al. The scenario model intercomparison project (scenariomip) for cmip6. *Geoscientific Model Development*, 9(9):3461–3482, 2016.

[19] O Gilard. Flood risk management: risk cartography for objective negotiations,[in:] third ihp/iahs george kovacs colloquium, 1996.

[20] Pritisha Pandey and Sumit Dugar. Flood hazard mapping in an urban context: A case study of hanumante stream, bhaktapur (nepal). In *Proc. IOE Grad. Conf*, volume 6, pages 435–444, 2019.

[21] Daniel N Moriasi, Jeffrey G Arnold, Michael W Van Liew, Ronald L Bingner, R Daren Harmel, and Tamie L Veith. Model evaluation guidelines for systematic quantification of accuracy in watershed simulations. *Transactions of the ASABE*, 50(3):885–900, 2007.

[22] Md Monirul Islam and Kimiteru Sado. Development priority map for flood countermeasures by remote sensing data with geographic information system. *Journal of hydrologic engineering*, 7(5):346–355, 2002.

[23] Bhakta Shrestha. Assessment of flood hazard and agriculture damage under climate change in the bagmati river basin of nepal. *International Journal of Environment*, 8(2):55–69, 2019.

[24] Nigel W Arnell and Simon N Gosling. The impacts of climate change on river flood risk at the global scale. *Climatic Change*, 134:387–401, 2016.